IEEE Access
Multidisciplinary ⋮ Rapid Review ⋮ Open Access Journal

Received 15 October 2025, accepted 30 October 2025, date of publication 4 November 2025, date of current version 18 November 2025.

Digital Object Identifier 10.1109/ACCESS.2025.3628903

RESEARCH ARTICLE

Gentle Grasping: A Method With Low-Cost Magnetic Tactile Sensors

YI LIU, REMKO PROESMANS, (Member, IEEE), ANDREAS VERLEYSEN, AND FRANCIS WYFFELS

IDLab-AIRO, ELIS, IMEC, Ghent University, 9000 Ghent, Belgium

Corresponding author: Yi Liu (yiyiliu.liu@ugent.be)

ABSTRACT Human tactile capabilities enable the manipulation of various objects seamlessly in everyday life. We present a grasping strategy employing a two-fingered parallel gripper with a low-cost magnetic tactile sensor. The sensor provides three-dimensional force feedback during the grasping process. Using the tactile sensing, we can detect slip during the object's lift phase. We propose a force approximation technique that dynamically adjusts force increments to identify the critical slip threshold of objects. This allows the robot to maintain a stable grasp on the threshold where an unknown object is about to slip. We validated our approach through experiments involving 20 diverse everyday objects. The results demonstrate that our slip detection based on low-cost magnetic tactile sensors is effective and that the proposed force approximation method swiftly determines the critical slip threshold for various everyday objects.

INDEX TERMS Robotic grasping, sensor-based control, linear slip detection, various objects manipulation.

I. INTRODUCTION

Human grasping relies on the skin's tactile feedback, enabling precise handling of objects with diverse properties such as stiffness and weight. Replicating the tactility of the human skin for robots is difficult, and grasping the mentioned types of objects with a few tactile sensors is a challenge.

Perception is a key factor in robotic grasping, which can provide environmental feedback to the robot to ensure that the robot can complete the corresponding task [1]. Among the key perceptual modalities in grasping are vision and touch. Vision provides information of the object's state, including texture, volume, position, and material. This can help to locate the object and perform grasping [2]. However, vision alone is insufficient for perceiving physical interactions with objects. To address this limitation, recent approaches have integrated vision and touch to enhance grasping performance [3], [4]. In these methods, tactile feedback is used to assess the state of the object within the robot's grip and adjust hand posture accordingly.

Tactile sensors are crucial in robotic grasping, as they provide feedback on an object's state during the grasping process [5], [6]. Three-dimensional tactile sensors, which can detect both normal and shear forces, are essential for a more comprehensive understanding of object interactions compared to one-dimensional pressure sensors [7]. Magnetic tactile sensors [8], [9] and capacitive tactile sensors [10], [11] can obtain 3D information. However, their signal outputs often exhibit coupling. The methods to decouple this 3D information include special structural designs [12] and stacking piezoresistive sensors on magnetic sensors [13]. Simple sensors are employed in compression tasks [10], and 3D sensors are used in lifting tasks to detect slip [12], [14]. The complexity of the tactile sensor design depends on the sensing needs. One-dimensional sensors can be constructed using basic varistors, whereas 3D sensors often involve intricate manufacturing processes [15]. For example, the study in [13] utilizes magnetic tactile sensors to detect object slip, enhancing their functionality by layering capacitive sensors over the magnetic sensing points to address signal coupling issues inherent in magnetic tactile sensors. Therefore, tactile sensing grasping based on rich information is considered.

Grasping unknown objects requires robots to be adaptive, including the ability to adapt to the object's shape [16], [17] and position [18]. For unknown physical properties of objects, some studies have used force feedback data to perform grasping [19]. Compared with the geometric properties of objects, the unknown physical properties of an object are

The associate editor coordinating the review of this manuscript and approving it for publication was Mauro Fadda.

more complex, diverse and difficult to observe [4]. Therefore, unknown geometric properties as well as physical properties are considered. The basic controller is the driver for robot interaction with unknown objects [20]. Grasping objects with varying characteristics requires precise force control to prevent slippage or damage. There are several ways to control a robot remotely using a compliant controller [21], [22], but we need to accomplish autonomous control of the robot. A possible approach is to apply fracture prediction to find the force boundaries that cause the object to deform or break [23]. Another (safer) approach is to control the force on the slip boundary. There are multiple methods for slip detection [24], [25], [26]. Some studies have considered identifying the geometry of the object to adjust the grasping posture [16], [18], but they do not consider the physical properties of the object, such as whether it can be destroyed. Some work uses neural networks to train robots to randomly grasp unknown objects [27]. Some works use tactile feedback information to render the physical properties of unknown objects [4]. For gentle grasping, some algorithms have been developed to achieve this goal [28]. Some studies designed the teleoperation framework with a compliant controller [20], [22], however, teleoperation is a human-based strategy to control the robot, which disables the autonomy of the robot. Various studies have employed machine learning methods to train robots for grasping tasks [29], [30], integrating visual and tactile information. However, the sparsity of tactile data can negatively impact its effectiveness in the context of data-driven models, e.g., when directly inputted into neural networks. To mitigate this, some approaches preprocess tactile data before using it as input, though this still necessitates the collection of training data. Some works used the characteristics of tactile sensors to design simple controllers to achieve gentle grasping [31]. Alternatively, adaptive control methods have been used to perform grasping tasks [32]. These methods adjust the hand posture in real-time based on sensory information, ensuring robust and gentle grasping without the need for pre-trained data.

In this work, we focus on force change-based slip detection [33], which is simpler to deploy and avoids the complexities associated with data-driven slip detection methods [34]. As shown in Fig. 1, we deploy a low-cost 3D tactile fingertip for slip detection. A force control algorithm based on an admittance controller is implemented. Constrained grasping is utilized to effectively handle objects with unknown properties (e.g., stiffness, weight, brittleness). We use force approximation to adjust the applied force dynamically, ensuring secure and adaptable grasping performance across a wide range of objects.

The contributions of this paper are summarized as follows:

1) We introduce a versatile grasping framework that leverages low-cost 3D magnetic tactile sensors for the manipulation of everyday objects, providing a practical solution for integrating tactile sensing into robotic fingertips;

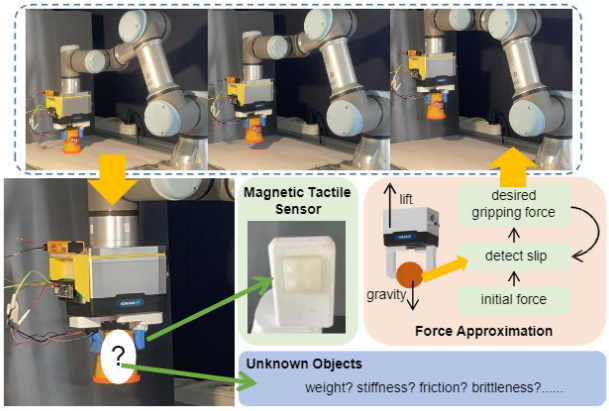

FIGURE 1. The overall grasping strategy. Detecting slip through the feedback of the magnetic tactile sensors, and using force control to grasp objects with unknown properties (e.g., weight, stiffness, brittleness).

2) We present a force control strategy that accurately determines the slip boundary during the lifting phase. This ensures that the object does not break or undergo significant deformation;
3) The proposed force control method is thoroughly tested on diverse everyday objects.

II. METHODOLOGY

The control algorithm we proposed is described in this section, which includes a basic admittance controller, a proposed slip detection method, and a proposed force approximation method for grasping.

A. MAGNET-BASED SENSORS

In this study, we employed a fingertip with four magnetic 3D force sensing taxels in a 2-by-2 grid [35]. The three-dimensional force information is crucial for precise slip detection during grasping. The readout system allows for robust and real-time feedback, essential for implementing our force control algorithm based on the admittance controller.

At the heart of the fingertip design, shown in Fig. 2(a), lies a printed circuit board (PCB) with a 2-by-2 grid of MLX90393 Hall effect sensors connected through an I^2C bus. A dome structure similar to [36] and [37] is printed in Flexible FLGR02 resin using a Formlabs Form 2 printer. Cylindrical magnets with a height of 1 mm and diameter of 1.5 mm are superglued into the domes, and the dome structure itself is glued to the PCB. A cover for the PCB is 3D printed in PLA using a Prusa i3 MK3. A smooth contact surface is cast onto the cover using Silicone Addition Colorless 50 by Silicones and More. Fig. 2(b) shows the moulding setup. Crucially, a mock PCB is inserted into the cover during curing. The domes on the mock PCB are shorter than the resin domes. This way, when the mock PCB is removed and the resin domes are inserted after curing, an air gap surrounds each dome. The air gap ensures that the force applied to the silicone surface is transferred to the resin domes. Finally, the cover is

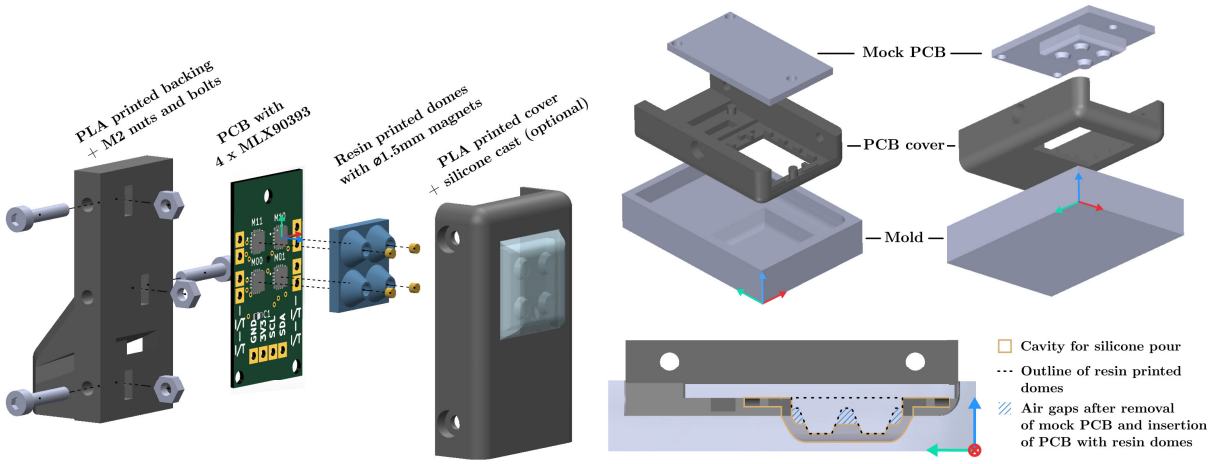

(a) Fingertip structure. The magnets are glued into the domes, the domes are glued onto the PCB. The PCB is pressed between the cover and backing, and the cover is bolted to the backing.

(b) Mould for silicone pour. The domes on the mock PCB are shorter than the resin-printed domes, such that after removal of the mock PCB and insertion of the PCB with resin domes, an air cavity is present all around each dome.

FIGURE 2. Mechanical structure of the tactile fingertip.

bolted to a PLA backing (Fig. 2(a)). The backing is designed to fit a Robotiq 2F-85 gripper.

The sensor is calibrated by fixing the PCB to a UR3e robot arm, manually deforming the domes in different directions and recording both the Hall sensor readings and the force-torque (F/T) readings of the UR3e. For each taxel, polynomial features up to the third degree are extracted from the Hall readings. An 80%/20% train-test split is randomly sampled and a least squares linear regressor is fitted on the train set. The result is a model per taxel that takes in the X, Y and Z components of the magnetic field and predicts the three components of the force applied to the taxel. This calibration procedure, however, does not take the silicone contact surface into account. Hence, there is some coupling between the normal and shear force readings, which will be accounted for in our slip detection algorithm (see sections II-C and III-B). For clarity, we conduct a comparative analysis between our method and recent baselines, including magnetic and capacitive tactile sensors as well as gentle grasping controllers. The comparison highlights key differences in sensor type, slip detection strategy, and control approach, as summarized in Table 1.

B. TACTILE-BASED CONTROLLER

The magnet-based tactile sensors deployed on the fingers provide real-time feedback on the contact status of the fingers. This feedback allows the robot to adjust the position of the fingers. An admittance controller effectively manages the relationship between force and position, and its basic model is expressed as follows:

$$M_{\mathrm{d}}(\ddot{x}_{\mathrm{d}} - \ddot{x}_0) + D_{\mathrm{d}}(\dot{x}_{\mathrm{d}} - \dot{x}_0) + K_{\mathrm{d}}(x_{\mathrm{d}} - x_0) = f_{\mathrm{tac}} - f_{\mathrm{d}}, \quad (1)$$

where x_{d}, $\dot{x}_{\mathrm{d}}$, $\ddot{x}_{\mathrm{d}}$ represent the desired position, desired speed and desired acceleration of the finger, respectively. x_0 in mm, $\dot{x}_0$ in mm/s, $\ddot{x}_0$ in mm/s^2 represent the current position, current speed and current acceleration of the finger, respectively. f_{d} in N denotes the desired grasping force in z-axis direction, i.e. the pressing direction. f_{tac} in N represents tactile feedback. M_{d}, D_{d}, K_{d} correspond to the inertia, damping and stiffness characteristics of the finger respectively. All the parameters above are scalar (one-dimensional) quantities.

The relationship between force and position in the admittance controller is determined by the physical properties (M_{d}, D_{d}, K_{d}) of the finger. Given that the observed value f_{tac} is explicit, we only need to define the physical properties for the finger. Then, we can control the finger's position based on tactile feedback to achieve the desired grasping force.

C. SLIP DETECTION

Pure force control cannot achieve our goal of grasping objects with different properties because f_{d} in Equation 1 is unknown. Therefore, the f_{d} is discussed in this section, and a slip detection method is proposed to detect whether the object is stably grasped.

Above all, for slip detection, we broadly classify the objects based on stiffness attributes into three categories: rigid objects, deformable objects, and fragile objects. As shown in Fig. 3, we only consider the force feedback of the object and the idealized curve is shown. There is a slip boundary of force f_{s} for all objects, which is used to determine whether the object is slipping. There is a breaking boundary of force f_{b} for fragile objects, which is used to determine whether the object is destroyed. To facilitate idealized explanation, we set the same f_{s} and f_{b} for all objects. It should be noted that the slip force f_{s} and the breaking force f_{b} are distinct physical quantities. The same values shown in Fig. 3 are only

TABLE 1. Comparison of the proposed method with recent tactile sensing and gentle grasping approaches.

Method	Sensor Type	Cost	Calibration Effort	Slip Metric	Control Policy
Proposed	Magnetic	Low	Minimal	Real-time, adaptive	Adaptive gentle grasping
AnySkin [8]	Magnetic	High	High	Fixed force threshold	Feedback control
GelSight [39], [40]	Optical	High	High	Deformation vector field	Feedback control
TacTip [17], [41]	Optical	Medium	High	Machine learning-based	Support vector machine
Soft Capacitive [5], [11]	Capacitive	Medium	Medium	Machine learning-based	Adaptive grasping
Barometric [42]	Barometric	Low	Low	Machine learning-based	Slip detection

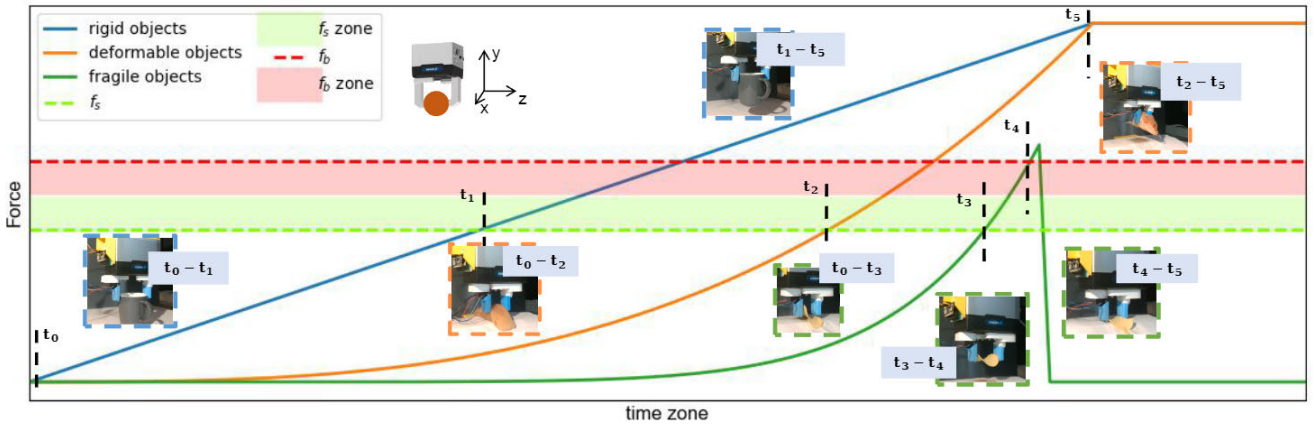

FIGURE 3. Ideal diagram of the grasping force for rigid objects, deformable objects, and fragile objects. Rigid objects do not deform, deformable objects deform elastically, fragile objects may deform both elastically and plastically. f_d is defined as the desired force for grasping the objects, f_s is the slip boundary, and f_b is the break boundary. Different objects have different f_s and f_b. Each curve represents the lifting process of an object, starting from initial time t_0. For the gripper, the z-axis is the pressing direction, and the y-axis is the lifting direction. The progression of grasping in different time zones for each type of object is shown. f_s zone represents the upper area near the slip boundary, and f_b zone represents the lower area near the breaking boundary. The ideal f_d is inside the f_s zone and close to f_s.

used for idealized illustration purposes. In general, $f_s < f_b$. When the f_d used by the object is less than f_s, the rigid objects (t_0–t_1), deformable objects (t_0–t_2) and fragile objects (t_0–t_3) slip. When $f_d > f_s$, the rigid objects (t_1–t_5) and deformable objects (t_2–t_5) can be grasped. Particularly, the fragile objects (t_3–t_4) can be grasped with a force between f_s and f_b, when $f_d > f_b$, the fragile objects (t_4–t_5) break. To grasp the object without breaking it, f_s obtained by slip detection is considered to be the f_d of the object. However, we cannot get the precise f_s, so we set f_s zone and f_b zone. In this way, we need to control f_d in f_s zone to ensure that the object can be grasped without crossing f_b zone and being destroyed. In particular, for unknown objects, their f_s and f_b zones are unknown. Since our proposed framework requires grasping unknown objects and needs to consider multiple properties of objects (volume, stiffness, brittleness, etc.), data-based estimation methods are not in our consideration. In order to achieve gentle grasping, we adopt a force approximation approach such that the force applied to the object is in the f_s zone (details are shown in II-D), which is regarded as a dynamic estimation of the f_s zone. As shown in Fig. 3, an object is destroyed when the applied force exceeds the f_b zone, which is not the purpose of this paper, so we do not estimate the value of f_b zone for all objects.

In addition, we constrain the grasping direction to be aligned with the lift direction, i.e. the y-axis as shown in Fig. 3. Grasping along the x-axis could lead to collisions with the table surface for small objects. Since a two-finger gripper is used for lifting, we do not consider slip detection in the rotational direction. Furthermore, this constraint reduces the impact of coupling in the sensor readings on slip detection: the coupling between the normal and both shear force directions is different, so the measured f_s and f_b thresholds depend on the slip direction. However, this pragmatic approach does not diminish the applicability of our grasping method.

Referring to the detection method of [12], the changing relationship between the forces in the y-axis and z-axis directions f_y/f_z is considered as a metric for slip detection. Due to the effect of coupling, we consider the derivative f_y/f_z as $\Delta f_y/\Delta f_z$. This is because when an object slips or falls off, the force change in the y-axis direction is larger than that in the z-axis direction, and the value of $\Delta f_y/\Delta f_z$ can sensitively determine whether it is slipping. The slip metric s_c is represented as

$$s_c = \begin{cases} 1, & \Delta f_y/\Delta f_z < o_s \\ 0, & \text{otherwise,} \end{cases} \tag{2}$$

where o_s expresses the threshold approaching zero. Since we use a parallel two-finger gripper and consider the slip direction of the y-axis, objects can only slip downwards ($\Delta f_y/\Delta f_z < o_s$) in the y-axis direction due to insufficient force when lifting.

D. APPROXIMATION METHOD FOR DESIRED FORCE

With the purpose of obtaining f_d for each object, an approximation method based on incremental force is considered. Since the characteristics of the object to be grasped are unknown, first of all, the initial grasping force f_0 is considered, and the force step δf is set to adjust the current force to make it close to f_d. It can be expressed as

$$\hat{f}_d(t) = f_0 + \sum_{i=1}^{t} s_c \delta f_i, \tag{3}$$

where $\hat{f}_d$ in N represents the desired force at the time t. The f_0 is a small fixed value for initialization. We add the second item $\sum_{i=1}^{t} s_c \delta f_i$ to make f_d close to the f_s zone. In particular, the tactile sensor has four taxels to increase the contact area and cover the entire finger, hence, the force $\hat{f}_d$ we choose is the average feedback value of the tactile sensor points during the grasping process.

To speed up the approximation, we consider adjusting δf to a dynamic value. The $\alpha_d = |\Delta f_y / \Delta f_z|$ from the slip detection is taken into account as a factor to adjust δf. At the lifting stage, the f_y increases, and f_z increases slightly as well due to the coupling factor but not as fast as f_y. Therefore, α_d and δf are positively correlated, expressed as

$$\delta \hat{f} = e^{\alpha_d}, \tag{4}$$

where $\delta \hat{f}$ represents the desired δf. Since the force feedback of some objects, such as deformable objects, is nonlinear, we make $\delta \hat{f}$ have a large adjustment when α_d is large and slightly adjust when α_d is small, similar to the nonlinear modeling of the soft bodies [42], the Euler's number e is considered as the heuristics factor for nonlinear mapping between $\delta \hat{f}$ and α_d. To prevent $\delta \hat{f}$ obtained from exponential explosion, we constrain the range of α_d to be within $[\alpha_s, \alpha_e]$ and map δf to $[\delta f_s, \delta f_e]$, which are expressed as $\alpha_d \in [\alpha_s, \alpha_e]$ and $\delta \hat{f} \rightarrow [\delta f_s, \delta f_e]$.

Furthermore, the stiffness of the object is a factor for speeding up the grasping process. The difference p_e between the finger's initial position p_i and current position p_c when grasping is used as a mapping of stiffness. For objects with high stiffness, small deformation occurs during grasping, so stiffness and p_e are negatively correlated. To prevent soft objects from being squeezed and deformed, we define a nonlinear mapping as a positive correlation between stiffness and δf. Similar to slip detection, the Euler's number is considered as the factor for nonlinear mapping [43], Equation 4 is rewritten as

$$\delta \hat{f} = e^{\alpha_d} + \frac{1}{e^{p_e}}, \tag{5}$$

where the second term expresses that an object with high stiffness uses greater force, and vice versa for an object with low stiffness. Similar to α_d, the constraint of range $p_e \in [p_{es}, p_{ee}]$ is given. In particular, Euler's number in Equ. 4 and Equ. 5 is a heuristic parameter to make the function nonlinear, and their final mapping results are artificially constrained to prevent the value of the force $\delta \hat{f}$ change at each step from being too large.

Finally, the change in f_y during the lifting stage affects the f_z in II-A. To allow the system to control f_z in the normal direction as much as possible, we give switching constraints. We obtain the historical f_z for one second to calculate the average $\overline{f_z}$. If $\overline{f_z}$ is greater than $\hat{f}_d$, replace the existing value of $\hat{f}_d$. Equation 3 is rewritten as

$$\hat{f}_d(t) = \begin{cases} f_0 + \sum s_c \delta f, & \overline{f_z} \le \hat{f}_d(t-1) \\ \overline{f_z}, & \overline{f_z} > \hat{f}_d(t-1). \end{cases} \tag{6}$$

The approximation method proposed initiates the grasping force at f_0 and adjusts it by δf during the lifting process.

Algorithm 1 Grasping Process

Require:
initialize grasping posture P_{arm} and δf
$f_d = f_0$; $P_{arm} = P_i$; $\delta f = 0$; $n = 100$; $t = 0$;

// n is the number of sampled data in the past 1 second;

while *True* **do**
  Let P_{arm} move to the target in the child thread
  $t = t + 1$
  $p_e(t) = p_i - p_c(t)$
  $\alpha_d(t) = |\Delta f_y(t) / \Delta f_z(t)|$
  $f_d(t) = f_d(t-1) + s_c(e^{\alpha_d(t)} + 1/e^{p_e(t)})$
  $\overline{f_z} = \sum_{k=1}^{n} f_z(k)/n$
  if $\overline{f_z} > f_d(t)$ **then**
    $f_d(t) = \overline{f_z}$
  end if
  $x_d(t) \leftarrow$ *Equation 1* $\leftarrow (f_{tac}(t) - f_d(t))$
end while

For intuitive explanation, the overall flow of Algorithm 1 is demonstrated. The objective of this paper is to make f_d approach the slip boundary f_b zone of the unknown object, so that the unknown object can be gently grasped. Therefore, we initialize the gripper's posture and some parameters in preparation for grasping. Then, we assume that the stiffness of all objects is an elastic system, and we calculate the distance p_e that the finger moves during the grasping process to represent the stiffness of the object. Finally, we combine p_e and the slip detection metric α_d to update the desired force f_d based on the heuristic Equ. 5, which is used to correct the admittance controller in II-B to adjust the finger position x_d. Although Algorithm 1 does not directly take brittleness f_b or f_s as inputs, it operates under this classification, adjusting the grasping force search process depending on whether a breaking boundary f_b is considered (for fragile objects) or not (for rigid/deformable objects). All in all, the proposed algorithm uses the slip detection metric and the stiffness information of the object to approximate the force of the grasping process to

adjust the finger position. It can adapt to the physical properties of unknown objects and make dynamic adjustments according to the unknown slip boundary f_s zone of the object.

III. EXPERIMENTS AND RESULTS

To achieve our methodology, we constructed both slip detection and grasping experiments. The slip detection experiments were conducted to compare different detection metrics. For the grasping experiments, we employed the proposed approximation method described in Section II-D to determine the grasping force and designed the corresponding ablation experiment.

A. EXPERIMENTAL SETUP

All experiments were conducted using the UR3e robot equipped with a Schunk-EGK-40 gripper. The gripper communicated with the laptop via RS-485, and we deployed the tactile fingertip described in section II-A on one side of the gripper. The sampling frequency of the sensor was 100 Hz, and its feedback was calibrated to a value in *Newtons*, the details about the sensor's calibration matrix, cross-axis errors and simulation studies can be seen in the previous work [35]. The control frequency of the gripper was 50 Hz. Since we had constraints in the lifting direction (II-C), the contact area between the fingers and the object during the lifting process was not large, so we set the manipulator to pull up slowly at a constant speed of 1 mm/s during the lifting process.

For ease of understanding, we provided the necessary configuration for the method. In II-B. The finger's inertia characteristic was set to $M_d = 1$. For high damping and low-stiffness compliance, the damping and stiffness parameters were set to $K_d = 5, D_d = 5$, respectively. These settings were based on tactile sensor feedback, ensuring the gripper could stably grasp objects with the ideal force. The displacement variables in the admittance controller were all converted from the position, and the sampling frequency was 50 Hz. In II-C, the threshold o_s and the initial force f_0 were both set to approach zero. We defined $o_s = f_0$, meaning that if the change in grasping force between t and $t+1$ exceeded the value of initial force, it indicated a slip. The f_0 was slightly larger than the minimum force feedback value of the tactile sensor. For all experiments, we collected four seconds of sensor data in the released state to obtain the maximum noise n_i, and added 0.05 (the number close to zero) to make f_0 valid, resulting in $f_0 = n_i + 0.05$. In addition, the α_d and $\delta\hat{f}$ were the positive numbers in Equation 4. α_d directly constrained the value range, while $\delta\hat{f}$ constrained the mapping range after calculation. The range of α_d was, from the slip detection boundary ($\alpha_s = o_s$) to the maximum limit ($\alpha_e = 1$), expressed as $\alpha_d \in [o_s, 1]$. $\delta\hat{f}$ is mapped to prevent excessive force, defined as multiples of $\delta\hat{f} \rightarrow [f_0/5, f_0/2]$. Similarly, p_e was limited to the minimum movement distance ($p_{es} = 0.01\ mm$) and maximum movement distance ($p_{ee} = 10\ mm$), which was expressed as $p_e \in [0.01, 10]$. The initial grasping posture P_t was fixed so the gripper always grasped the same position, but objects were artificially placed at random within a graspable range.

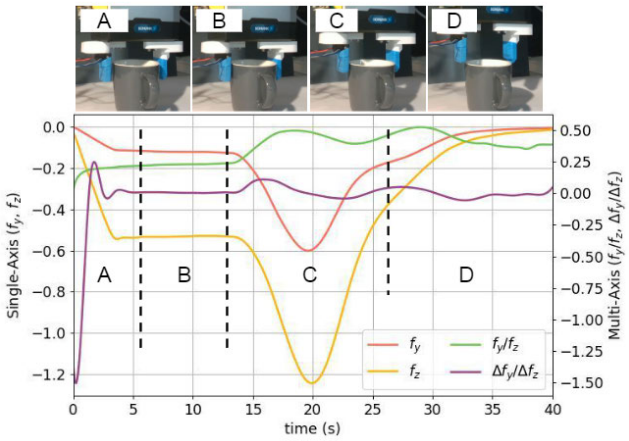

FIGURE 4. Slip detection metrics. We used a heavy rigid body as an object to test the performance of force feedback. The unit of force is *Newton*. The curve includes the process from initialization to the end of grasping (A→D).

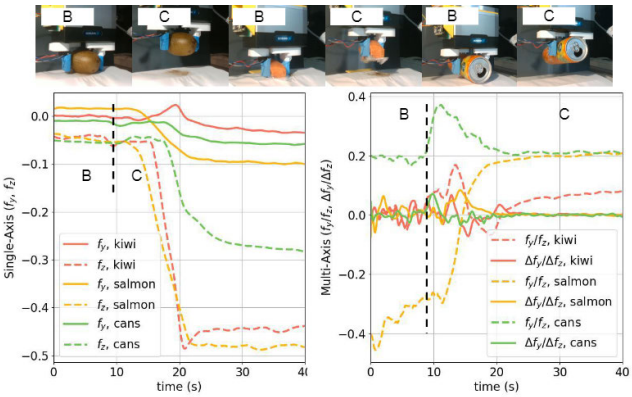

FIGURE 5. Grasp feedback performance for multiple objects. We tested three different types of objects to observe the difference in the slip detection metrics of different objects. The unit of force is *Newton*. It showed the closing (B) and lifting (C) stages of the objects. The left curve represents. The curve on the left represents the force feedback value of the single axis of the sensor, and the curve on the right represents the change between the two axes.

B. SLIP DETECTION EXPERIMENT

The coupling of the low-cost magnetic tactile sensors required evaluating the force on the sensor in multiple directions in order to detect slip. Our goal is to distill the required features that indicate slip. We did not consider data-driven approaches that require pre-collected data. II-C provided movement direction constraints, so we focused on forces in the y-axis and z-axis directions, such as $f_z, f_y, f_y/f_z, \Delta f_y/\Delta f_z$. Then, we utilized the same object as the test target and tried to lift the object once when f_z was stable. Ensuring the object was not lifted allowed us to compare different slip detection metrics.

To prevent the manipulator from lifting the object, we chose a heavy object, a mug filled with metal. As shown

in Fig. 4, for the object (mug) during lifting with $f_d = 0.55$ N, different slip detection metrics were given. We illustrated four stages of the grasping process: finger opening at initialization (A), closing (B), lifting (C), and releasing (D), where zone C indicated the force approached zero due to slip. The corresponding zones were marked on the curve, with zones B and C being the main focus for slip detection. In zone B, the fingers began to close and grasp the object stably with f_d. Due to the coupling of the sensor, the value in the y-axis direction changed as well. Therefore, the coupled f_y was not used as the metric for slip detection. Similarly, coupled f_z could not be used as the metric as well. f_y/f_z and $\Delta f_y/\Delta f_z$ did not change much in zone B, because f_y and f_z were stable. In zone C, due to slip, the value of f_y changed more than f_z one, and the value of f_y/f_z began to increase, $\Delta f_y/\Delta f_z$ increased at the same time. When the slip distance was too large, the object began to slip out of the hand. f_y/f_z approached zero, the value of $\Delta f_y/\Delta f_z$ decreased at the same time. f_y/f_z needed to be greater than the slip boundary f_s to be considered non-slip in Fig. 3, and we could not obtain the exact value of f_s for all of the objects, hence, the derivative $\Delta f_y/\Delta f_z$ and f_s were considered as metric of the slip detection. In zone D, the finger had already left the object. However, because the surface of the tactile sensor was covered with silicone, the deformed silicone caused the tactile sensor value to return to zero slowly instead of immediately. Because we can detect whether the object slip using the metric $\Delta f_y/\Delta f_z$ and f_y/f_z in zone C, the zeroing curve of zone D was not within our consideration.

We obtained two different metrics for slip detection by lifting a heavy object, which could definitely make the finger slip. Finally, for further comparison (f_y/f_z vs. $\Delta f_y/\Delta f_z$), as shown in Fig. 5, we utilized the proposed force approximation method to perform a grasp of different objects, demonstrating that the slip boundaries varied among them. We tested the performance on a kiwi, salmon, and cans, focusing primarily on the holding and lifting processes. For unknown objects, the proposed method lifted all of the objects in zone C, but the values of f_y/f_z in zone C were different, indicating that slip boundaries differed among objects. Additionally, $\Delta f_y/\Delta f_z$ was near zero before entering zone C, showing that f_y/f_z had stabilized. However, it changed in zone C, indicating slip. The method we proposed needed to grasp unknown objects, and for different objects, their slip boundaries f_s were different, which means we could not define a fixed slip boundary for all objects. In contrast, the metric $\Delta f_y/\Delta f_z$ for different objects fluctuated around zero during the grasping process and after stable grasping, which met the requirements of the method we proposed. Therefore, $\Delta f_y/\Delta f_z$ better reflected the slip of different objects than f_y/f_z. In particular, the gentle grasping we implement in this paper does not take into account the rotation of the object (mentioned in II-C), making use of f_y/f_z as a detection metric of the y-axis direction is simple and effective, but its form is single, and can not be widely promoted. We can see that the reason it doesn't consider feedback on the x-axis is that the direction of lift is on the y-axis. Similar to [12], we can use the cross-product of the y and x-axis to replace f_y for a limited generalization. However, this type of generalization ability is limited and needs to consider factors such as the weight of the object, so we do not use it as a comparison metric.

C. FORCE APPROXIMATION EXPERIMENT

We designed the experiment to compare different methods. First (G1, III-C1) grasped all objects with a fixed grasping force. Second (G2, III-C2) utilized the proposed method with a fixed force step δf to grasp the objects. Third (G3, III-C3) grasped the objects with the force approximation method. As shown in Fig. 6, we performed 20 daily items and their different states, a total of 28 items as grasping targets for the experiment. We defined the classification of objects as fruits (id_{1-9}), food ingredients (id_{10-14}), snacks (id_{15-19}), meats (id_{20-25}) and daily cups (id_{26-28}) based on a single attribute for discussion. The three methods were used as ablation experiments to compare the impact of δf on the proposed model. We tested all objects 15 times to obtain the grasping success rate s_r, the time t_g required for grasp stabilization, and the grasping force f_g of various objects. The success rate s_r was defined as successfully picking up the object without destroying or losing it, and the grasping force f_g was the average value of the sensor obtained for 4 seconds after grasping was successful. t_g was the time required from f_0 to f_g during lifting.

The setup details for each experiment (shown in Table 2) were as follows,

1) FIXED GRASPING FORCE (G1)

In the G1 experiment, we used a fixed grasping force to lift objects. We set the force to $f_{\text{fixed}} = 1$ N and modified Equation 3 to $\hat{f}_d = f_{\text{fixed}}$. We removed the admittance controller and the re-grasping part from Algorithm 1. Since the force $\hat{f}_d$ was fixed, breaking an object was considered a failure, and we did not consider the f_g and t_g because the force was not controlled when lifting.

2) FIXED FORCE STEP APPROXIMATION (G2)

The G2 experiment followed the grasping process of Algorithm 1, but with a fixed δf and without the re-grasping rule. To grasp objects with minimal force, we set δf to the minimum value in the specified range: $\delta f = f_0/5$.

3) DYNAMIC FORCE STEP APPROXIMATION (G3)

The G3 experiment utilized the complete grasping process of Algorithm 1 without the re-grasping rule, accelerating the search for the object's slip boundary force through dynamic δf.

As shown in Fig. 7, we displayed images of the grasping process of experiment G1, G2 and G3 of one representative object from each category mentioned by III-C. Videos of the grasping process of each object and all methods were provided in the video link. As shown in Fig 8, the test results for all of the objects were given, which included the results of

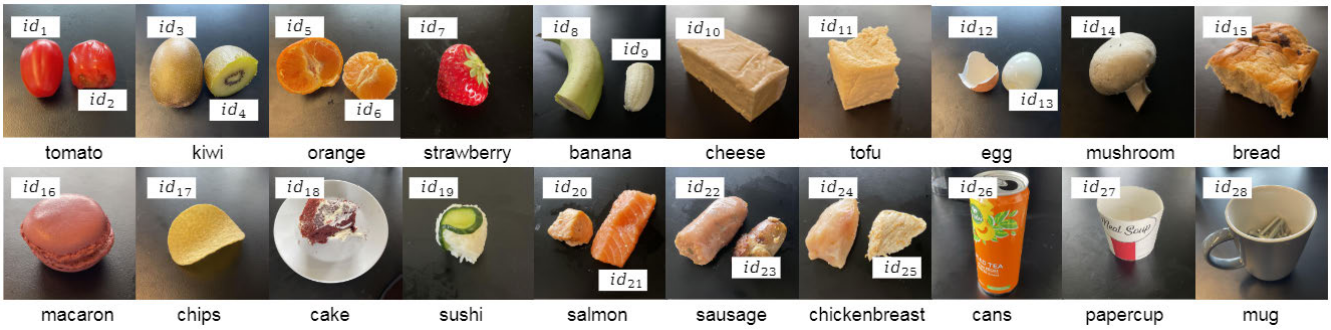

FIGURE 6. Everyday objects for grasping. We tested common objects in daily life such as foods, fruits, cups, and their different states (e.g. cooked, cut, rared). The names of the objects are marked in the picture, and the identification represents different states.

TABLE 2. Comparison of the three force determination methods (G1–G3).

Method	Constituents	Constraints	Assumptions	Limitations
G1	Constant grasping force $f_{\text{fixed}} = 1$ N; modified Equation 3 as $\hat{f}_{\text{d}} = f_{\text{fixed}}$.	Only contact and lifting zones; no re-grasping or adaptive control; no inequalities applied.	1 N is sufficient for stable lifting.	Not adaptable to different object properties, which leads to fragile objects breaking or heavy objects slipping.
G2	Incremental force update with constant $\delta f = f_0/5$; follows Algorithm 1.	Sequential discrete force zones; no re-grasping; ensures $f_{\text{tac}} < \hat{f}_{\text{d}}$ before each update.	Constant step provides a balance between stability and convergence.	Sensitive to δf choice; requires many steps for optimal grasp.
G3	Adaptive δf updated from tactile feedback and slip tendency.	Divides contact into pre-contact, stable, and slip zones; enforces $\hat{f}_{\text{d}}(t+\Delta t) \geq \hat{f}_{\text{d}}(t)$.	Tactile feedback accurately indicates slip onset.	Performance depends on sensor quality and feedback delay.

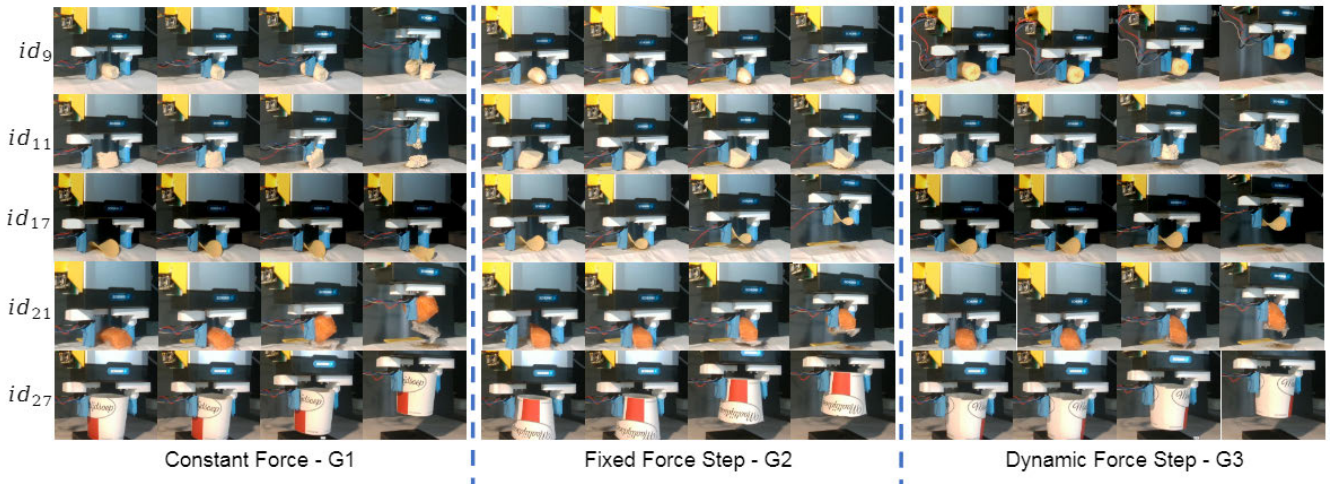

FIGURE 7. Object grasping process. We divided it into three parts, representing the performance of G1, G2 and G3 respectively. We only show some representative objects, including fruits, food, meat and cups. The performance of all objects was shown in the video link.

all mentioned methods, where the unit of f_{g} in *Newtons*, and the unit of t_{g} in *seconds*. We recorded the average number of successful grasping cases for f_{g} and t_{g}. Grasping of unknown objects mainly focused on the physical properties of the objects. As shown in Fig. 9, we selected four objects (orange, potato chip, cake, and fish) based on weight, brittleness, and stiffness/deformability, and demonstrated their performance in G2 and G3 methods, which include the approximation process of f_d and the feedback f_y and f_z of the tactile sensors.

D. DISCUSSION

In III-B, we compared different slip detection metrics and have discussed that $\Delta f_{\text{y}}/\Delta f_{\text{z}}$ was the best metric among all the discussed detection metrics. Hence, the slip detection metric

we used in III-C was $\Delta f_y/\Delta f_z$, and in this section we mainly discussed the results of the grasping experiments presented in III-C. including the comparison of s_r, f_g and t_g and the performance of grasping different unknown objects.

1) SUCCESS RATE

We utilized the three methods (G1, G2, G3) to perform the grasping attempt. In Fig. 7, we showed the grasping process of some objects. We could see that the objects (id_9, id_{11}, id_{17}, id_{21}) grasped by G1 method were destroyed due to excessive force. Compared with G1, G2 did not destroy the objects, but because the fixed force step δf was small, some objects (id_9, id_{11}) failed to be grasped. In G3, δf was dynamically adjusted, allowing objects that failed to be grasped in G2 to be successfully grasped in G3.

We showed the s_r of the test in Fig. 8, the G1 could successfully lift objects that would not be destroyed, such as whole fruits (id_1, id_3, id_5, id_8), meat (id_{22}, id_{23}) and daily cups (id_{26}, id_{27}), but it failed to grasp objects that were fragile (id_5, id_7, id_{11}, etc.). Compared to the G1, the G2 improved the success rate for grasping objects like fruits and snacks, enabling the grasping of objects that G1 could not handle. The difference between them was that the f_d used by G1 was a fixed value, while the f_d used by G2 was progressive, which allows G2 to grasp objects with a force in the f_s zone mentioned in Fig. 3, while the force used by G1 had exceeded the f_b zone for fragile objects. On the other hand, the G3 further increased success by using dynamic δf compared with the G2 one, showing that this approach enhanced grasping capabilities. For fragile objects such as id_{18} and id_{20}, although it could not achieve good results like other objects' performance, the performance was significantly improved compared to G2.

2) GRASPING FORCE AND TIME

For the impact of δf, we mainly compared G2 and G3 to analyze the grasping efficiency. We showed the f_g and t_g of all test objects in Fig. 8. For G1, f_g was around 1 N because the desired force we set was $f_d = 1$ N and the feedback value was close to 1 N. Therefore, since G1 did not adjust f_d, we would not discuss G1 in this section.

We could see that the grasping force of G3 was generally greater than that of G2, but G3 did not destroy the objects. This was because G3 used a more aggressive way to obtain δf, allowing the system to grasp the object quickly. Combined with s_r, G3 obtained a higher grasping success rate with slightly greater δf, and their variance of f_g was smaller than that of G2, indicating that the force of each grasped object fluctuated in a small range. On the other hand, grasping efficiency was considered. The t_g required by G2 was generally greater than that required by G3, which meant that the grasping efficiency of G3 was higher than that of G2. In particular, for t_g, the variance of G3 was greater than G2 one, because δf at each grasp changed, resulting in inconsistent t_g, while δf of G2 was fixed, resulting in similar t_g for each grasp. For different objects, f_g and t_g showed different values. For fragile objects (such as id_{12}, id_{18}, id_{20}), they could be grasped with a force less than 0.5 N. Due to their lower weight, snacks required less force. Compared with the intact object (such as id_1), the cut object (such as id_2) required less force because their surfaces were damaged and more easily deformed.

For a comprehensive comparison, we compared a method [44] that learns the f_b zone of an object with a low-cost setup by collecting forces during the process of squeezing the object leading to its destruction. They tested tofu (id_{27}), potato chips (id_{17}), and bananas (id_9) with success rates of 87.72, 87.42, and 85.98, respectively. The success rate is similar to our results. They used precision to represent the time it takes to grasp, and give an average time of 6.53 seconds for success in the case of tofu, which is much longer than ours. It can be seen that a high grasping success rate can be achieved on a low-cost setup, but our proposed method can quickly approach the desired f_s zone and perform gentle grasping.

To sum up, a fixed δf (G2) can facilitate the robot to find the slip boundary of an unknown object, while a dynamic δf (G3) can speed up the process of the former. Intuitively, when the object is grasped, the force applied to it changes from small to large, and the object should slip first and then be destroyed (shown in Fig. 3), therefore, the desired force obtained by G3 is in the f_s zone, that is, the minimum force with which an unknown object can be stably grasped.

3) UNKNOWN PHYSICAL PROPERTIES

Grasping a variety of unknown objects required adapting the hand to a variety of physical properties. The physical properties of all tested objects vary. We showed representative objects in Fig. 9 to discuss the adaptability of the proposed method to some physical properties.

As shown in Fig. 9, compared with method G2, the force f_d generated by G3 was larger, which was consistent with the discussion results of Fig. 8. The time for f_d of G3 to reach stability was shorter than that of G2, which showed that its acceleration to obtain an approximate f_d was effective. Then, G1's f_d was fixed and not shown. G1's f_z remained near 1 N, which showed that it always used fixed force to grasp objects. Similarly, f_z of G2 and G3 was controlled by f_d, so its value was close to f_d.

We were mainly concerned with whether the object can be grasped safely, so we want to keep f_g in the f_s zone mentioned in Fig. 3. Therefore, the f_g in Fig. 9 can be seen as a dynamic estimate of the f_s zone of an unknown object, reflecting the differences between the objects. We focused on the weight, brittleness, and deformability of objects. Among the four objects, id_{17} had the lightest weight, id_{21} had the strongest ductility, i.e., deformability, id_{18} was brittle, and id_5 was with peel, not easy to deform, and heavy. As can be seen from Fig. 9, for f_d, id_5 required a large force (0.6 N) to grasp, while the light-weight id_{17} only needed 0.15 N. In particular, for id_{21}, due to its strong deformability, it needed to be grasped with a large force (0.5 N). To verify the superiority of G3, we conducted a Wilcoxon signed-rank test [45] between G2

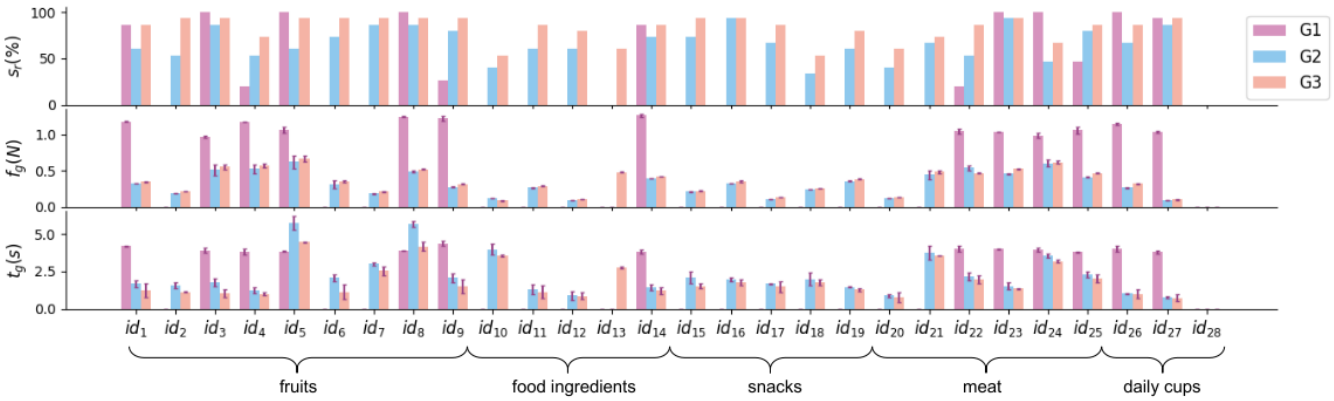

FIGURE 8. All objects test results. We divided objects into fruits, food ingredients, snacks, meat and daily cups. We recorded the test success rates of G1, G2 and G3 and the grasping data (the grasping force f_g for G1 was always 1 N). The t_g was the time required from f_0 to f_g during lifting. The heavy object mug used in the sliding detection experiment was used in this experiment, but it could not be lifted in all methods.

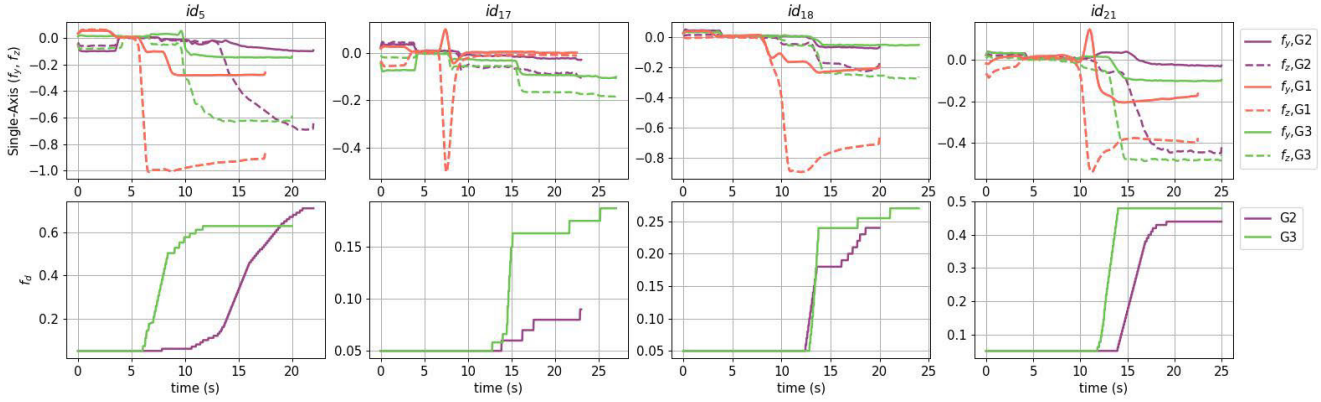

FIGURE 9. Grasping process of unknown objects. The unit of force is *Newton*. In order to demonstrate the efficiency of the proposed method G3, we gave the performance of the same object in the G2 experiment (G2 vs. G3). We selected unknown objects with greatly different physical properties for demonstration. For instance, the orange was the heaviest, the fish was highly deformable, the cake was fragile, the chips were crisp, etc. Since the desired force f_d of method G1 was fixed (1 N), it was not shown in the figure.

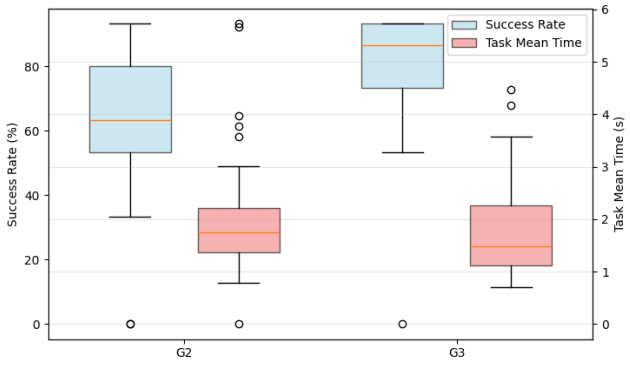

FIGURE 10. Comparison of the performance between models G2 and G3 across unknown objects. Blue boxes represent success rates, while red boxes represent task mean times. The Wilcoxon signed-rank test shows that G3 achieves significantly higher success rates and lower mean times ($p < 0.05$), indicating overall performance improvement.

and G3 based on the results shown in Fig. 9. As illustrated in Fig. 10, the p-value for the success rate was 0.00032, and the p-value for the task mean time (t_g) was 0.00020. Both values are below the significance threshold of 0.05, indicating that G3 exhibits a statistically significant performance improvement over G2.

Then, we discussed the exploration effects of all methods on the f_s zone and f_b zone of unknown objects. Referred to [12], to compare different objects, the f_s and f_b mentioned in Fig. 3 were assumed as f_z/f_y with no unit to make the schematic reasonable. For id_5, the G1 could work, which meant its real f_d was below 1 N but was not determinable. The f_s obtained by G1 was 3.35. Similarly, the f_s obtained by G2 was 7.13, and G3's f_s was 6.41. Since the object had not been destroyed, we could not get the object's f_b. For id_{17}, the G1 method broke the object and stopped working when a force of 0.5 N was applied. Therefore, we could get the object's f_b as 5.07 at the rupture point. The f_s obtained using G2 was 4.55, and G3's f_s was 2.94. It could be seen that the f_b of the highly brittle object (id_{17}) was close to the f_s of the tough object (id_5), which meant that the boundary f_b of the highly brittle object was low and it was easy to be destroyed. For id_{18}, the G1 destroyed the object, but the object did not break

into pieces like id_{17}. The G1's f_b was 3.87, the G2's f_s was 2.71, and the G3's f_s was 3.15. Similar to the case of id_{18}, for id_{21}, the G1's f_b was 5.30, the G2's f_s was 4.66, the G3's f_s was 4.71. Since G1 damaged the object, we primarily compared G2 and G3. We could observe that for fragile and deformable objects (id_{18}, id_{21}), the f_z/f_y of G3 was close to that of G2. For highly brittle objects (id_{17}), the f_z/f_y of G3 was significantly smaller than that of G2, indicating that G3 was closer to the f_s zone. Similarly, for high-mass objects, the f_z/f_y of G3 was smaller than that of G2. Overall, the results suggested that among the three methods, G3 could grip objects with a force closest to the f_s zone, which was the safest.

In short, the proposed force approximation method could be utilized as a method to gently grasp everyday objects. The G3 increased grasping efficiency compared to G2 and successfully grasped objects. For unknown objects with small f_z, the proposed method could also grasped them gently and efficiently.

IV. CONCLUSION AND FUTURE WORK

This paper introduces a force approximation method with slip detection leveraging low-cost 3D magnetic tactile sensors. Our approach focuses on using the slip boundary force as a target to ensure stable and non-destructive grasping of arbitrary objects. At the outset, we select the force of the slip boundary as the target force to ensure the proposed model can grasp objects without destroying or losing them. Then, we constrain the grasp direction to avoid slip detection in the rotation direction and select the slip detection metric to ensure that the low-cost coupled magnetic tactile sensor can be properly utilized. We use a single metric $\Delta f_y/\Delta f_z$ which is sufficient to measure slip since it accounts for the coupled force dimensions. In addition, a force approximation method based on slip detection method is proposed for grasping objects with unknown properties. The method was validated on a physical robot, testing it with 20 everyday objects. The results indicate that our approach effectively grasps objects with unknown properties, in particular, it can achieve gentle grasping of objects with the low f_b boundary or soft objects, demonstrating its practical applicability and robustness.

However, there are limitations to our current implementation. Specifically, the constrained grasping direction limits the system to a single grasping action. Future work will address this limitation by extending the method to support grasping from any direction and add slip detection in the rotation direction, enhancing the system's versatility and generalization. Additionally, for objects that are challenging to grasp such as heavy objects, we plan to improve the grasping rules, aiming to achieve successful grasps. Finally, we use a two-finger gripper, which has a single action. We can use multi-degree-of-freedom fingers instead to improve the flexibility of the robot. Moreover, a data-driven grasping strategy will be introduced as a stronger baseline to enhance adaptability across diverse object types and contact conditions. To ensure safety and stability during grasping, a hard force cap will be incorporated to prevent excessive contact force.

REFERENCES

[1] A. Roychoudhury, S. Khorshidi, S. Agrawal, and M. Bennewitz, "Perception for humanoid robots," *Current Robot. Rep.*, vol. 4, no. 4, pp. 127–140, 2023.

[2] B. Huang, S. D. Han, J. Yu, and A. Boularias, "Visual foresight trees for object retrieval from clutter with nonprehensile rearrangement," *IEEE Robot. Autom. Lett.*, vol. 7, no. 1, pp. 231–238, Jan. 2022.

[3] F. Zhu, R. Jia, L. Yang, Y. Yan, Z. Wang, J. Pan, and W. Wang, "Visual-tactile sensing for real-time liquid volume estimation in grasping," in *Proc. IEEE/RSJ Int. Conf. Intell. Robots Syst. (IROS)*, Oct. 2022, pp. 12542–12549.

[4] Q. Feng, Z. Chen, J. Deng, C. Gao, J. Zhang, and A. Knoll, "Center-of-Mass-based robust grasp planning for unknown objects using tactile-visual sensors," in *Proc. IEEE Int. Conf. Robot. Autom. (ICRA)*, May 2020, pp. 610–617.

[5] S. Ergun, T. Mitterer, S. Khan, N. Anandan, R. B. Mishra, J. Kosel, and H. Zangl, "Wireless capacitive tactile sensor arrays for sensitive/delicate robot grasping," in *Proc. IEEE/RSJ Int. Conf. Intell. Robots Syst. (IROS)*, Oct. 2023, pp. 10777–10784.

[6] Z. Zhou, Z. Zhang, K. Xie, X. Zhu, and Q. Cao, "A brief review focused on tactile sensing for stable robot grasping manipulation," in *Intelligent Robotics and Applications*, 2022, pp. 628–639.

[7] C. Han, Z. Cao, Y. Hu, Z. Zhang, C. Li, Z. L. Wang, and Z. Wu, "Flexible tactile sensors for 3D force detection," *Nano Lett.*, vol. 24, no. 17, pp. 5277–5283, May 2024.

[8] R. Bhirangi, V. Pattabiraman, E. Erciyes, Y. Cao, T. Hellebrekers, and L. Pinto, "AnySkin: Plug-and-play skin sensing for robotic touch," in *Proc. IEEE Int. Conf. Robot. Autom. (ICRA)*, May 2025, pp. 16563–16570.

[9] A. Pagoli, M. Alkhatib, and Y. Mezouar, "A soft variable stiffness gripper with magnetorheological fluids for robust and reliable grasping," *IEEE Robot. Autom. Lett.*, vol. 9, no. 5, pp. 4519–4526, May 2024.

[10] T. Yao, X. Guo, C. Li, H. Qi, H. Lin, L. Liu, Y. Dai, L. Qu, Z. Huang, P. Liu, C. Liu, Y. Huang, and G. Xing, "Highly sensitive capacitive flexible 3D-force tactile sensors for robotic grasping and manipulation," *J. Phys. D, Appl. Phys.*, vol. 53, no. 44, Oct. 2020, Art. no. 445109.

[11] K.-H. Ha, H. Huh, Z. Li, and N. Lu, "Soft capacitive pressure sensors: Trends, challenges, and perspectives," *ACS Nano*, vol. 16, no. 3, pp. 3442–3448, Mar. 2022.

[12] Y. Yan, Z. Hu, Z. Yang, W. Yuan, C. Song, J. Pan, and Y. Shen, "Soft magnetic skin for super-resolution tactile sensing with force self-decoupling," *Sci. Robot.*, vol. 6, no. 51, p. 8801, Feb. 2021.

[13] H. Meng, W. Zhu, L. Zhou, X. Qian, and G. Bao, "A 3-D force sensor based on combination of magnetic and piezoresistive transduction," *IEEE Sensors J.*, vol. 22, no. 4, pp. 3595–3604, Feb. 2022.

[14] B. Fang, Z. Xia, F. Sun, Y. Yang, H. Liu, and C. Fang, "Soft magnetic fingertip with particle-jamming structure for tactile perception and grasping," *IEEE Trans. Ind. Electron.*, vol. 70, no. 6, pp. 6027–6035, Jun. 2023.

[15] M. Li, T. Li, and Y. Jiang, "Marker displacement method used in vision-based tactile sensors—From 2-D to 3-D: A review," *IEEE Sensors J.*, vol. 23, no. 8, pp. 8042–8059, Apr. 2023.

[16] C. Eppner and O. Brock, "Grasping unknown objects by exploiting shape adaptability and environmental constraints," in *Proc. IEEE/RSJ Int. Conf. Intell. Robots Syst.*, Nov. 2013, pp. 4000–4006.

[17] R. Zenha, B. Denoun, A. Cavallaro, A. Bernardino, and L. Jamone, "Let's DENSE: A novel protocol for efficiently collecting dense and diverse data for tactile slip detection in robotic grasping," *npj Robot.*, vol. 3, no. 1, p. 36, Oct. 2025.

[18] M. Kiatos, S. Malassiotis, and I. Sarantopoulos, "A geometric approach for grasping unknown objects with multifingered hands," *IEEE Trans. Robot.*, vol. 37, no. 3, pp. 735–746, Jun. 2021.

[19] C. Wang, X. Zhang, X. Zang, Y. Liu, G. Ding, W. Yin, and J. Zhao, "Feature sensing and robotic grasping of objects with uncertain information: A review," *Sensors*, vol. 20, no. 13, p. 3707, Jul. 2020.

[20] A. Weiss, A.-K. Wortmeier, and B. Kubicek, "Cobots in Industry 4.0: A roadmap for future practice studies on Human–Robot collaboration," *IEEE Trans. Human-Mach. Syst.*, vol. 51, no. 4, pp. 335–345, Aug. 2021.

[21] P. N. Dao, V. Q. Nguyen, and H. A. N. Duc, "Nonlinear RISE based integral reinforcement learning algorithms for perturbed bilateral teleoperators with variable time delay," *Neurocomputing*, vol. 605, Nov. 2024, Art. no. 128355.

[22] P. N. Dao, N. T. Dang, T. L. Nguyen, and G. K. Dinh, "Finite-time sliding mode control strategies for perturbed input-constrained nonlinear bilateral teleoperation systems with variable-time communication delays," *Intell. Service Robot.*, vol. 18, no. 2, pp. 363–378, Mar. 2025.
[23] R. Yagawa, R. Ishikawa, M. Hamaya, K. Tanaka, A. Hashimoto, and H. Saito, "Learning food picking without food: Fracture anticipation by breaking reusable fragile objects," in *Proc. IEEE Int. Conf. Robot. Autom. (ICRA)*, May 2023, pp. 917–923.
[24] Y. Liu, J. Zhang, Y. Lou, B. Zhang, J. Zhou, and J. Chen, "Soft bionic gripper with tactile sensing and slip detection for damage-free grasping of fragile fruits and vegetables," *Comput. Electron. Agricult.*, vol. 220, May 2024, Art. no. 108904.
[25] Z. Xie, T. Piriyatharawet, and C. Roberto, "Deep learning LSTM-based slip detection for robotic grasping," in *Proc. IECON 49th Annu. Conf. IEEE Ind. Electron. Soc.*, Oct. 2023, pp. 1–5.
[26] S. Cui, J. Wei, X. Li, R. Wang, Y. Wang, and S. Wang, "Generalized visual-tactile transformer network for slip detection," *IFAC-PapersOnLine*, vol. 53, no. 2, pp. 9529–9534, 2020.
[27] H. Zhang, J. Peeters, E. Demeester, and K. Kellens, "A CNN-based grasp planning method for random picking of unknown objects with a vacuum gripper," *J. Intell. Robotic Syst.*, vol. 103, no. 4, pp. 1–19, Dec. 2021.
[28] K. Kleeberger, R. Bormann, W. Kraus, and M. F. Huber, "A survey on learning-based robotic grasping," *Current Robot. Rep.*, vol. 1, no. 4, pp. 239–249, Dec. 2020.
[29] Q. Bai, S. Li, J. Yang, Q. Song, Z. Li, and X. Zhang, "Object detection recognition and robot grasping based on machine learning: A survey," *IEEE Access*, vol. 8, pp. 181855–181879, 2020.
[30] D.-J. Boonstra, L. Willemet, J. Luijkx, and M. Wiertlewski, "Learning to estimate incipient slip with tactile sensing to gently grasp objects," in *Proc. IEEE Int. Conf. Robot. Autom. (ICRA)*, May 2024, pp. 16118–16124.
[31] C. J. Ford, H. Li, J. Lloyd, M. G. Catalano, M. Bianchi, E. Psomopoulou, and N. F. Lepora, "Tactile-driven gentle grasping for human-robot collaborative tasks," in *Proc. IEEE Int. Conf. Robot. Autom. (ICRA)*, May 2023, pp. 10394–10400.
[32] P. Lynch, M. F. Cullinan, and C. McGinn, "Adaptive grasping of moving objects through tactile sensing," *Sensors*, vol. 21, no. 24, p. 8339, Dec. 2021.
[33] P. Kyberd, "Slip detection strategies for automatic grasping in prosthetic hands," *Sensors*, vol. 23, no. 9, p. 4433, Apr. 2023.
[34] J. Liu, J. Xie, S. Huang, C. Wang, and F. Zhou, "Continual learning for robotic grasping detection with knowledge transferring," *IEEE Trans. Ind. Electron.*, vol. 71, no. 9, pp. 11019–11027, Sep. 2024.
[35] L. V. d. Stockt, R. Proesmans, and F. wyffels, "Automatic calibration for an open-source magnetic tactile sensor," in *Proc. ViTac Workshop at Int. Conf. Robot. Autom. (ICRA)*, 2024.
[36] T. P. Tomo, M. Regoli, A. Schmitz, L. Natale, H. Kristanto, S. Somlor, L. Jamone, G. Metta, and S. Sugano, "A new silicone structure for uSkin—A soft, distributed, digital 3-axis skin sensor and its integration on the humanoid robot iCub," *IEEE Robot. Autom. Lett.*, vol. 3, no. 3, pp. 2584–2591, Jul. 2018.
[37] P. Sathe, A. Schmitz, T. P. Tomo, S. Somlor, S. Funabashi, and S. Shigeki, "FingerTac–An interchangeable and wearable tactile sensor for the fingertips of human and robot hands," in *Proc. IEEE/RSJ Int. Conf. Intell. Robots Syst. (IROS)*, Oct. 2023, pp. 10813–10820.
[38] W. Yuan, S. Dong, and E. Adelson, "GelSight: High-resolution robot tactile sensors for estimating geometry and force," *Sensors*, vol. 17, no. 12, p. 2762, Nov. 2017.
[39] N. Jawale, N. Kaur, A. Santoso, X. Hu, and X. Chen, "Learned slip-detection-severity framework using tactile deformation field feedback for robotic manipulation," in *Proc. IEEE/RSJ Int. Conf. Intell. Robots Syst. (IROS)*, Oct. 2024, pp. 13569–13576.
[40] B. Ward-Cherrier, N. Pestell, L. Cramphorn, B. Winstone, M. E. Giannaccini, J. Rossiter, and N. F. Lepora, "The TacTip family: Soft optical tactile sensors with 3D-printed biomimetic morphologies," *Soft Robot.*, vol. 5, no. 2, pp. 216–227, Apr. 2018.
[41] A. Grover, C. Grebe, P. Nadeau, and J. Kelly, "Under pressure: Learning to detect slip with barometric tactile sensors," 2021, *arXiv:2103.13460*.
[42] A. Pappalardo, A. Albakri, C. Liu, L. Bascetta, E. De Momi, and P. Poignet, "Hunt–crossley model based force control for minimally invasive robotic surgery," *Biomed. Signal Process. Control*, vol. 29, pp. 31–43, Aug. 2016.
[43] H. Inci, E. Selim, E. Tatlicioglu, E. Zergeroglu, and A. Savran, "A saturation based self-tuned robust control design for Euler Lagrange systems," *ISA Trans.*, vol. 156, pp. 565–578, Jan. 2025.
[44] R. Ishikawa, M. Hamaya, F. Von Drigalski, K. Tanaka, and A. Hashimoto, "Learning by breaking: Food fracture anticipation for robotic food manipulation," *IEEE Access*, vol. 10, pp. 99321–99329, 2022.
[45] W. J. Conover, *Practical Nonparametric Statistics*. Hoboken, NJ, USA: Wiley, 1999.

YI LIU received the M.Sc. degree, in 2021. He is currently pursuing the Ph.D. degree with the IDLab-AIRO, IMEC, Ghent University. His research interests include robotic intelligent control, machine learning, and human–computer interaction.

REMKO PROESMANS (Member, IEEE) received the M.Sc. degree, in 2016. He is currently pursuing the Ph.D. degree (with an expertise in the domain of tactile sensing and robotics) with the IDLab-AIRO, IMEC, Ghent University. His research interest includes the integration of low-dimensional tactile sensing in general-purpose robot manipulation.

ANDREAS VERLEYSEN received the M.Sc. and Ph.D. degrees, in 2014 and 2022, respectively. He began his career as an Optimization Consultant for a startup, where he spent three years on developing vehicle routing problem software. He is currently a Robotics and AI Specialist with the IDLab-AIRO, IMEC, Ghent University, with a passion for applying cutting-edge research to solve real-world challenges. He is driven by a love for technology and a desire to push the boundaries of innovation. He applies state-of-the-art research to create impactful, real-world applications. He is focused on bringing advanced robotics and AI solutions to industry, using the latest innovations in AI, sensing, motion optimization, on-edge signal processing, gripper design, and modeling to help companies and researchers develop the next generation of tomorrow's robot helpers.

FRANCIS WYFFELS received the M.Sc. and Ph.D. degrees, in 2007 and 2013, respectively. He is currently an Associate Professor with the IDLab-AIRO (airo.ugent.be), IMEC, Ghent University, with expertise in machine learning and robotics. Passionate about scientific outreach, he initiated educational projects and citizen-science initiatives. Through these activities, he aims to provide a realistic perspective on robotics and AI, foster inclusive STEM communities, and reduce the innate fear of robotics. His research interests include robot control through neural networks, multi-modal sensing for robots, and other robot helper technologies. He coordinated the robotic manipulation team of IDLab-AIRO that won the robotic folding competition track of the sixth and seventh Robotic Grasping and Manipulation Competition at IROS 2022 and ICRA 2023. Furthermore, he organized the ICRA 2024 Cloth Manipulation Competition.